CONTROLLING NICKEL NANOPARTICLE SIZE IN AN ORGANIC/METAL-ORGANIC MATRIX THROUGH THE USE OF DIFFERENT SOLVENTS

ADAM BERLIE, IAN TERRY AND MAREK SZABLEWSKI

ABSTRACT. Nickel nanoparticles have been created in an organic-based matrix by the reaction of $Ni(COD)_2$ (COD=1,5,-bis-cyclooctadiene) and 2,3,5,6-tetrafluoro-7,7,8,8- tetracyanoquinodimethane ($TCNQF_4$). The size of the nickel nanoparticles can be controlled by the use of different solvents and inclusion of tetrahydrofuran (THF) within the reaction to stabilise the Ni(0) atoms from the $Ni(COD)_2$. Materials are characterised with a combination of X-ray diffraction, electron microscopy and magnetometry and it is found that samples made using a halocarbon solvent resulted in clustered bulk Ni particles (size ≤ 10 nm) with anomalously high superparamagnetic blocking temperatures. Using an isocyanide solvent produces smaller (size ~ 1 nm), well dispersed particles that show little evidence of superparamagnetic blocking in the range of temperatures investigated (> 2 K). In all samples there is another component which dominates the magnetic response at low temperatures and shows an interesting temperature dependent scaling behaviour when plotted as M vs B/T which we believe is related to the organo-metallic matrix that the particles are trapped within. We propose that the enhanced blocking temperature of particles synthesised using halocarbon solvents can be attributed to inter-particle dipolar interactions and nanoparticle-matrix exchange interactions.

1. INTRODUCTION

There has been much interest in the synthesis of ferromagnetic materials based upon charge transfer salts consisting of transition metals and organic acceptors. Perhaps the most important material in this field to date is the amorphous bulk ferromagnet $V(TCNE)_x \cdot y(DCM)$, where $x \approx 2$ and $y \approx 0.5$ (TCNE = tetracyanoethylene; DCM = dichloromethane) [1]. This ferromagnetic material has a Curie temperature of over 400 K and it was suggested that in this charge transfer compound there was antiferromagnetic exchange between the donor and acceptor spins that resulted in a ferrimagnetic system [1]. It was also found that varying the solvents within metal-organic reactions can lead to dramatic effects and it was shown that T_C decreased with increasing polarity of solvent[1]; $V(TCNE)_x \cdot y(THF)$ (THF = tetrahydrofuran) shows a $T_C = 210$ K and $V(TCNE)_x \cdot y(CH_3CN)$ has a $T_C = 140$ K [2, 3, 4]. The reduction in transition temperature was attributed to the increased disorder induced by the more polar solvent. From x-ray diffraction studies the structural short range order is greater in the less polar solvent: DCM (25 Å), THF (15 Å) and CH_3CN (10 Å) [2, 3]. The increased randomness is due to the affinity of the solvent for the V(II) ion; THF and acetonitrile can bond with the magnetic ion via the oxygen and nitrile group respectively. If a solvent group is directly bonded to the vanadium then this will create a spinless spacer between the ions within the structure and interrupt the magnetic exchange. Since the isonitrile group is most effective at bonding to the vanadium it is no surprise that this shows the lowest T_C [4]. At low temperatures within all the solvent systems considered there is a glassy component and, although within $V(TCNE)_x \cdot y(DCM)$ the solvent does not influence the T_C, the disorder created does increase the effect of the spin glass phase.

More recently, it was reported that a novel high-temperature metal-organic ferromagnet ($T_C \geq 400$ K) could be synthesised by reacting bis-(1,5-cyclooctdiene) nickel ($Ni(COD)_2$) with the organic acceptors (A); 2,3-dichloro-5,6-dicyano-1,4-benzoquinone (DDQ), TCNE and 7,7,8,8-tetracyanoquinodimethane (TCNQ) to produce charge transfer salts Ni_2A, via a redox reaction,

---

[1]The polarities of the solvents used by Miller and Epstein in decreasing order: Acetonitrile, THF and DCM

using DCM as the solvent[5]. The Ni_2A systems were reported to be amorphous yet still show bulk ferromagnetic behaviour at room temperature similar to $V(TCNE)_x \cdot y(DCM)$, where $x \approx 2$ and $y \approx 0.5$ [1]. It was suggested that in this charge transfer compound there was antiferromagnetic exchange between the donor and acceptor spins that resulted in a ferrimagnetic system [1]. Miller *et al* further investigated the Ni_2A system by reacting $Ni(COD)_2$ with tetracyanoethylene (TCNE), in a 2:1 ratio and using the solvent tetrahydrofuran (THF). This reaction resulted in a mixed product material where it was suggested that one component consisted of Ni nanoparticles formed from the decomposition of $Ni(COD)_2$ and accounted for the remnant magnetization at room temperature. Another component was thought to be present was $Ni(TCNE)_2 \cdot THF$ which is a paramagnetic compound that displays magnetic ordering at low temperatures. Reacting the $Ni(COD)_2$ and TCNE in a 1:2 ratio resulted in a paramagnetic $Ni(TCNE)_2$ compound with a temperature independent magnetic component below 200 K [6].

The precursor used by Jain *et al*[5] and Miller *et al* [6] in their metal-organic redox reactions was $Ni(COD)_2$, which is a widely used material with many applications [7] such as in the creation of Ni nanoparticles. Such a process is effective due to the material's labile nature and its autocatalytic decomposition from Ni(0) to bulk Ni. There are many synthetic routes to control the decomposition, one of the simplest is probably applying energy to the system using sonication [8] which has been used to produce Ni particles encapsulated in carbon that behave superparamagnetically [9, 10]. Nanoparticles that are dispersed within a matrix can show some very interesting magnetic properties that are related to interactions between the moments on each particle. Competing interactions and changes in particle size can cause a system to show superparamagnetic, super spin glass or super ferromagnetic properties [11, 12, 13].

The uncertainty of the outcome of the interaction of nickel-cyclooctadiene with organic acceptor molecules has prompted us to investigate the reaction of $Ni(COD)_2$ with $TCNQF_4$ (2,3,5,6-tetrafluoro -7,7,8,8-tetracyanoquinodimethane), which is a derivative of TCNQ and behaves in a similar fashion in stabilising an anion radical. The reaction is a room temperature synthetic process and we have studied the effect of choice of solvent used during the synthesis on the materials produced. We find that, in all cases, the reaction results in Ni nanoparticles embedded within a metal-organic matrix. The Ni nanoparticle size can be controlled using different solvents with larger Ni particles of approximately 10 nm resulting from halocarbons while particle sizes of 1-2 nm were obtained when using isocyanide solvents. However, the magnetic properties of the reaction products are complicated by inter-particle interactions and by the response of the metal-organic matrix.
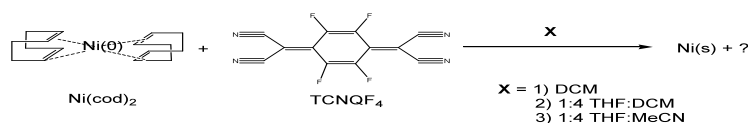
2. Experimental

Figure 1. Reacation scheme where **X** = DCM, THF/DCM, THF/MeCN, THF/DCB or THF/PhCN

$Ni(COD)_2$ (98+%) was purchased from Strem Chemicals UK and the $TCNQF_4$ (99.99%) was obtained from Durham Research and Synthesis. The solvents, identified in Fig. 1, were dried, degassed and stored under an inert atmosphere. The $TCNQF_4$ was dissolved in a solvent and added to the $Ni(COD)_2$ in a 1:2 ratio which produced a dark brown/black precipitate almost immediately except when using nitrile based solvents where a green intermediate was bypassed. All reactions were conducted under argon using a Schenk line and the ratios of solvents used are shown in Table 1. Note that THF was used to stabilise the $Ni(COD)_2$ so that decomposition did

not occur so rapidly, preventing bulk nickel formation and enhancing the chance of $Ni(COD)_2$ reacting with the $TCNQF_4$ to form a charge transfer system.

Sample	Ni(COD)$_2$ Solvent	TCNQF$_4$ Solvent	Ratio
1	-	DCM	-
2	THF	DCM	1:4
3	THF	MeCN	1:4
4	THF	DCB	1:4
5	THF	PhCN	1:4

TABLE 1. Solvents used in the reaction of $Ni(COD)_2$ and $TCNQF_4$. DCM = dichloromethane, THF = tetrahydrofuran, MeCN = acetonitrile, DCB = dichlorobenzene and PhCN = benzonitrile

Elemental analysis[2] was performed on a Dionex DX120 and ICPMS (Inductively Coupled Plasma Mass Spectroscopy)[3] was performed using a Perkin Elmer-Sciex Elan 6000; the results were used to obtain information on the compositions of each sample. An important parameter is the N:Ni ratio which gives the stoichiometry of the system and, assuming an ideal system of $Ni_2(TCNQF_4)$, one would expect N:Ni = 2:1. The compositional data of the five materials synthesised are shown in Table 2. Using these data we calculate the following N:Ni ratios; sample 1: 1.22:1; sample 2: 3.48:1; sample 3: 2.98:1; sample 4: 1.07:1; sample 5; 1.51:1. Clearly, all five samples do not agree with the $Ni_2(TCNQF_4)$ formula unit. In fact the following stoichiometries are suggested from these results: sample 1: $Ni_{3.3}(TCNQF_4)$; sample 2: $Ni_{1.2}(TCNQF_4)$; sample 3: $Ni_{1.3}(TCNQF_4)$; sample 4: $Ni_{3.7}(TCNQF_4)$; sample 5: $Ni_{2.7}(TCNQF_4)$.

Sample	1	2	3	4	5
Ni (%)	27.30	12.70	13.80	32.70	26.30
C (%)	25.05	35.94	39.04	24.91	31.32
H (%)	1.13	1.88	2.83	2.10	2.55
N (%)	7.97	10.54	9.82	8.32	9.48
Total (%)	61.45	61.06	65.49	68.03	69.65

TABLE 2. Table showing the elemental analysis of the samples. Ni content was determined using inductively coupled plasma mass spectroscopy (ICPMS).

Different experiments were undertaken to study both the structure and magnetic properties of the materials. A JEOL 2100F FEG Transmission Electron Microscope (TEM) was used to obtain TEM and Electron Energy Loss Spectroscopy (EELS) images of the samples for morphological and compositional studies. A Siemans D5000 with a Cu source was used record Powder X-Ray Diffraction (PXRD) patterns from each sample to gain further insight into the composition and crystallinity of the materials. Magnetic characterization was carried out using a Quantum Design Magnetic Properties Measurement System (MPMS) at magnetic fields of up to 5 T and in a temperature range of 2 K to 360 K.

3. RESULTS

3.1. **Physical Characterisation.** TEM and EELS compositional images for sample 1 are shown in Fig. 2. Particles are clearly visible and, at 70-80 nm, are relatively large; EELS revealed that these areas are very Ni rich. The EELS N map (Fig. 2.4) suggests that the majority of nitrogen (and hence organic material) in the sample resides between the particles (i.e. in the matrix). A similar conclusion is suggested when considering the EELS F map.

---

[2]Used to determine the carbon, nitrogen and hydrogen content

[3]Used to determine the nickel content

However, there is evidence for nickel within the matrix suggesting that it is a metal-organic compound albeit rich in organic material. The diffuseness of the particles in the TEM images for samples 1, 2 and 4 suggest that they are actually composed of agglomerates of smaller particles. High-resolution images for Sample 1 are shown in the additional information where one can identify crystalline regions however it is not possible to pin down particle sizes.
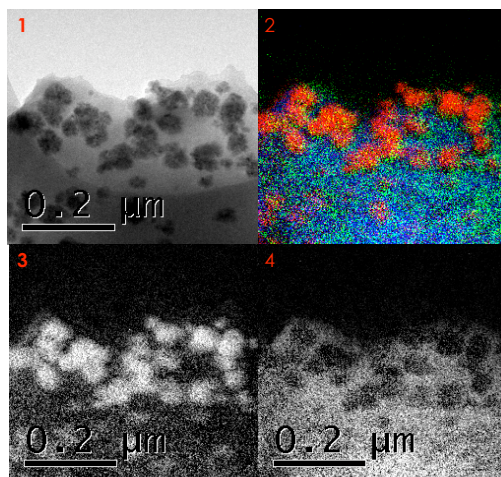

FIGURE 2. Sample 1 (solvent DCM) shows Ni rich areas within a crystalline matrix. 1) Elastic image; 2) overlay of EELS maps Red=Ni, Green=N and Blue=F ; 3) Ni map using EELS; 4) N map using EELS.

The TEM and EELS images for sample 2 (Fig. 3) are similar to those of Fig. 2 except the particle sizes are almost half those of the particles in sample 1. From the EELS images it is clear that these small particles are Ni rich and are probably Ni nanoparticles in an organic/metal-organic matrix. The images of both samples 1 and 2 suggest that the particles are clustering though this is less pronounced sample 2. Clustering in magnetic nanoparticulate systems is not uncommon and in many cases it is possible to see chaining of the particles or formations of rings so that there is flux closure [14, 15].
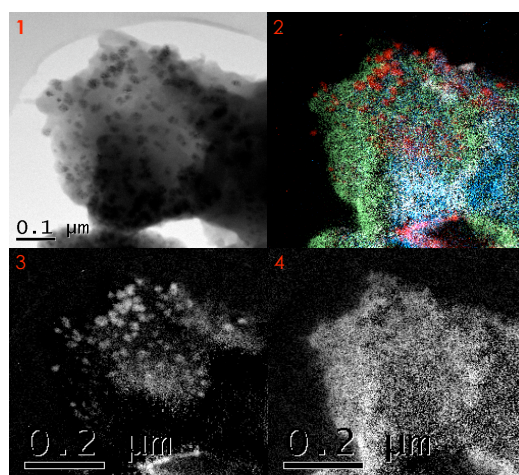

FIGURE 3. Sample 2 (solvent THF/DCM) also shows Ni rich areas. 1) Elastic Image; 2) overlay of EELS maps Red=Ni, Green=N, Blue=F and White=O; 3)Ni maps using EELS; 4) N map using EELS. *Note: The magnification in each image is the same however due to the switching over from the elastic imaging to EELS the default scale bar changes*

Sample 3 displays a radical difference to the previous two samples (Fig. 4). The particles are very small (< 5 nm) and appear to be very well dispersed within the matrix. Due to the small size of the particles it was not possible to perform EELS over a large area and we were confined to using only a 'spot' analysis. From the EELS spot analysis (Fig. 4.2) we found that there was a peak at 855 eV which corresponds to Ni suggesting that, although these particles are small, they are also Ni rich and most likely Ni nanoparticles. The Bright Field (BF) and High Angle Annular Dark Field (HAADF) images show the extent of this dispersion of the particles within the matrix.
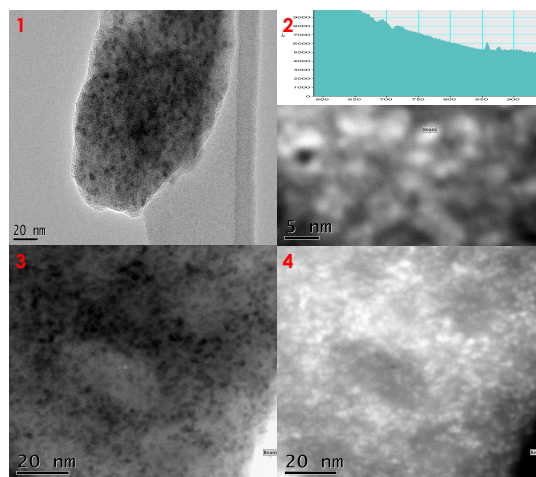

FIGURE 4. Sample 3 (solvent THF/MeCN). 1) Elastic image of area showing small particles 5 nm; 2) spot analysis using EELS of a particle in TEM image, graph (intensity vs. electron energy) shows peak at 855 eV which corresponds to Ni; 3) BF Image showing small particles; 4) HAADF image, the brighter areas have a higher Z number.

Fig. 5 shows a generic picture indicative of sample 4. Using DCB instead of DCM has produced a similar result to sample 1 though the particle sizes are much smaller and, from the EELS images, it is clear that the particles are very Ni rich; clearly we are observing the same type of material with Ni nanoparticles in an organic/metal organic matrix. Note that the N map (Fig. 5.4) suggests a nitrogen content that is more homogeneous than seen for samples 1 and 2 but this may be due to the imaged sample being quite thin with organic matrix above and below the nanoparticle regions.

Sample 5 (Fig. 6) is similar to sample 3 but it is only from the HAADF image that one can detect evidence for the existence of nanoparticles. The nanoparticles appear very well dispersed and the presence of a matrix is still detectable. Note that the nanoparticles are so small that it was not possible to perform any type of EELS to determine their composition, however, given the similarity to sample 3, it may be reasonable to assume that these particles are also Ni rich.

Powder x-ray diffraction experiments were performed on the different samples. Samples 1,2 and 4 all have characteristic face centred cubic (FCC) Ni peaks within the x-ray diffraction patterns as shown in figure 7 (reflections are indexed in the figure). The peaks are very broad due to the small nature of the Ni nanoparticles. From our data we use the Scherrer equation [16] to calculate the average particle size using the full width half-maximum of the peaks; the nickel particle sizes from the (111) peak at approximately $2\theta = 44.3°$ are 4.94 nm, 6.77 nm and 7.24 nm for samples 1, 2 and 4 respectively. This supports the conclusion from the TEM images that within these three samples the main component is nanoparticulate Ni, however at low angles there does appear to be structure that could be attributed to the metal-organic matrix. This is most prominent in sample 2, but there are some corresponding reflections in the
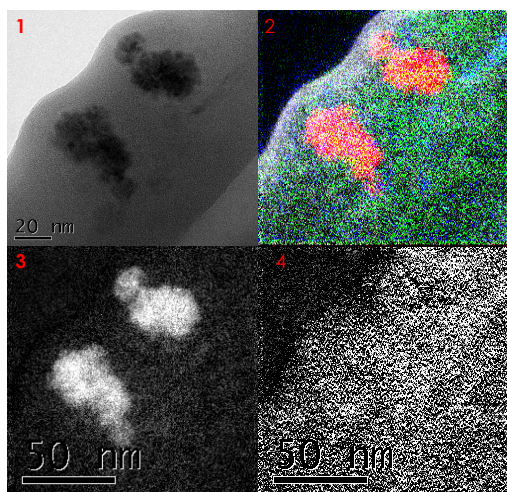
FIGURE 5. Sample 4 (solvent THF/DCB) shows the Ni rich areas within a matrix. 1) Elastic image; 2) overlay of EELS Maps Red=Ni, Green=N, Blue=F and White = O; 3) Ni Map using EELS; 4) N Map using EELS. *Note: The magnification in each image is the same however due to the switching over from the elastic imaging to EELS the default scale bar changes*
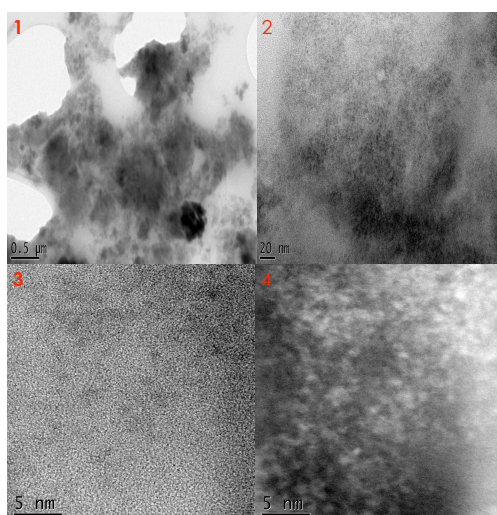

FIGURE 6. Sample 5 (solvent THF/PhCN) 1) Elastic image of area where there is no strong evidence for particles; 2) a close up image of the material where the darker areas may be Ni rich; 3) BF Image showing small particles; 4) HAADF image.

data of samples 1 and 4. In all three samples the peaks that do not match any phase of bulk Ni and, given the small values of 2θ, they may be associated with a structure that has large cell parameters e.g. a $TCNQF_4$ based material (there is no evidence to indicate the presence of bulk $TCNQF_4$ [17]).

The XRD patterns of samples 3 and 5 (figure 8) have no conclusive peaks that are directly associated with fcc Ni, although there may be some weak reflections at $2\theta \approx 50$ and $76°$, and, recalling the TEM images, this is consistent with very small particles (≤ 1 nm) that are dispersed throughout an organic matrix that is predominately a derivative of $TCNQF_4$. For comparison we include the XRD pattern of sample 2 in figure 8 and it can be seen that there is a general similarity between the peaks at small angles, once again suggesting the presence of a $TCNQF_4$
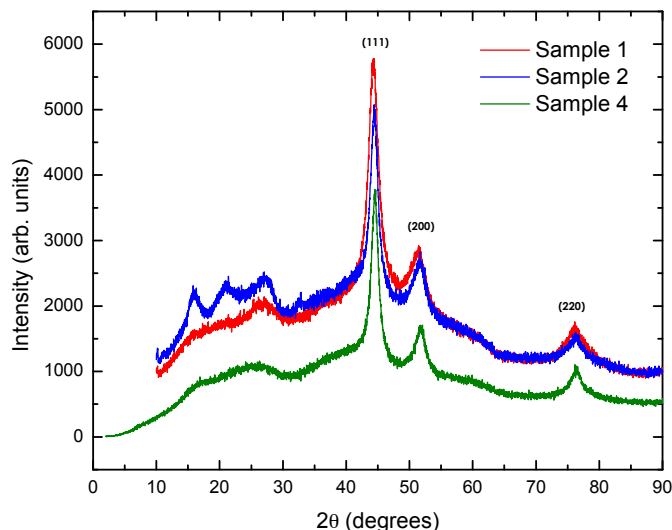
FIGURE 7. X-ray diffraction patterns for samples 1 (blue), 2 (red) and 4 (green). Sample 2 shows more structure at low angles than samples 1 and 4 indicating a more crystalline matrix or extra phase. The Ni reflections have been labelled on the graph.

derivative. It is hard to identify the specific material from the data at low angles (2θ) but it may be that the product is similar to those produced by Le *et al* [18, 19] from the electrochemical synthesis of Ni-TCNQF$_4$ compounds i.e. Ni(TCNQF$_4$)$_2$(H$_2$O)$_2$ or Ni(TCNQF$_4$)$_2$ (analogues of the paramagnet Ni(TCNQ)$_2$(H$_2$O)$_2$ [20] and ferromagnet Ni(TCNQ)$_2$ [21]). The XRD pattern associated with sample 5 suggests that it is very weakly crystalline/amorphous, with some diffuse peaks being observed but, from the TEM images (Fig. 6), there is evidence for very small particles that are most probably nickel and these particles may be too small (≤ 1 nm) to scatter the x-rays.
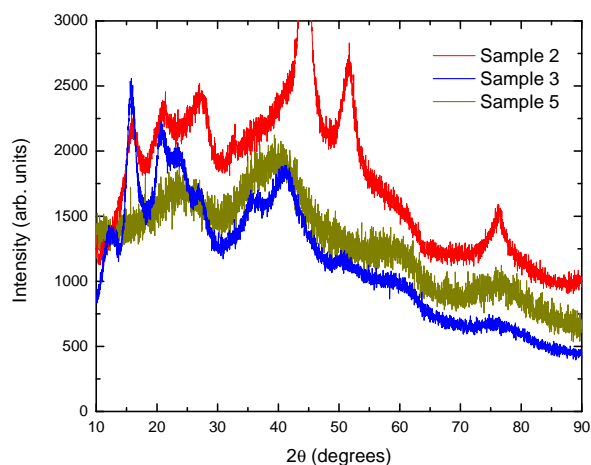

FIGURE 8. X-ray diffraction patterns for samples 3 (blue) and 5 (yellow). The PXRD data of sample 2 (red) has also been included for comparison of the low angle peaks.

The TEM, EELS and XRD data demonstrate that varying the solvent has a significant impact upon the creation of nickel nanoparticles through the decomposition of Ni(COD)$_2$. The general

similarity of samples 1, 2 and 4 suggests that neither DCM, nor THF with DCM or DCB, are able to prevent the decomposition process. The resulting materials are inhomogeneous with nickel nanoparticles embedded in a metal-organic matrix and the compositions, deduced from both elemental analysis and ICPMS, clearly do not represent the true nature of the samples. In fact the EELS maps of samples 1 and 2 indicate that the nickel content within the matrix is also very inhomogeneous implying a range of metal-organic compositions exist; the corresponding EELS map for sample 4 suggests that the matrix in this material has a very low nickel content even though the results of table 2 suggest that it is the most nickel-rich sample with respect to the nitrogen concentration. On the other hand the TEM and XRD data suggest that using the solvents THF and either acetonitrile or benzonitrile stabilises $Ni(COD)_2$ and, instead of following the decomposition path to form large nanoparticles of bulk nickel plus a metal-organic matrix, a more homogeneous material is synthesised; possibly a nickel salt with $TCNQF_4$ is formed via a charge transfer reaction. The role of the different polarities of solvents, and their effect on crystallinity, is discussed later.

3.2. **Magnetic Characterisation.** The magnetic properties of the five samples differ from each other though samples 1, 2 and 4 are similar and are vastly different to samples 3 and 5. Therefore we deal with these two groups of samples separately.

3.2.1. *Samples 1, 2 & 4.*
The Magnetization vs. Temperature data (Fig. 9) for the three samples, measured at 2.5 mT show a similar response to that expected for a superparamagnetic nanoparticulate system, though the FC data appearing to saturate as temperature is lowered. The individual blocking temperatures (T_B) vary between samples, as indicated in Table 3, which might be expected for nickel nanoparticles with differing sizes as $T_B \propto V$ where V is the volume of the superparamagentic particle [23]. However, PXRD data suggest that sample 1 has the smallest particle size, with sample 2 the next largest and sample 4 the largest; the blocking temperatures do not follow this trend. Also, the values for the FC magnetization at the lowest temperatures are similar for samples 1 ($M(4K) = 1.40$ Am^2kg^{-1}) and 4 ($M(4K) = 1.39$ $Am^{-2}kg^{-1}$), while that of sample 2 ($M(4K) = 0.88$ Am^2kg^{-1}) is rather different. Note the calculation of the magnetization was simply done by dividing the measured magnetic moment by the mass of the sample, and the TEM/EELS data demonstrated that the samples are inhomogeneous. Therefore the magnetic fraction of the samples responsible for the data of (Fig. 9) is not necessarily correctly represented by the bare masses of the samples used in the magnetic measurement. In fact, assuming all the nickel detected in the ICPMS measurement is responsible for the magnetic signal, and correcting the magnetization for this fraction of the mass, we obtain the following magnetizations at 4 K: sample 1, $M = 5.13$ Am^2kg^{-1}; sample 4, $M = 4.25$ $Am^{-2}kg^{-1}$; sample 2, $M = 6.93$ Am^2kg^{-1}.

Examining the blocking temperatures in more detail, we may calculate T_B using the a value of $K_1 = $ -4.5 x 10^3 Jm^3 [22] and the formula:

$$(1) \qquad\qquad T_B = KV/k_B \ln(\alpha t/\tau_0),$$

where $\alpha = 100$ and $\tau_0 = 10^{-9}$ s [23]. We used values of V from both PXRD (Scherrer equation) data and also deduced from the mean magnetic moments which are obtained fitting a Langevin function to M vs. H data at 290 K, which will be explained later. The measured and calculated values of T_B are given in Table 3 and it seen the calculated T_B values (for particles of the order of 7-10 nm) are about two orders of magnitude smaller than the blocking temperatures determined from Fig. 9. Note that the apparent particle sizes observed in the TEM data also do not correspond to the measured values of T_B supporting the idea the images are of aggregates of much smaller particles. The typical particle sizes calculated using T_B and those determined from M vs. H or PXRD data suggest that the matrix may be enhancing the the magnetocrystalline anisotropy of the nanoparticles through a modification of their surface magnetism. It has been previously observed that the blocking temperature in films of Ni nanoparticles within a matrix can be tuned depending on the material of the matrix and increased above what is expected
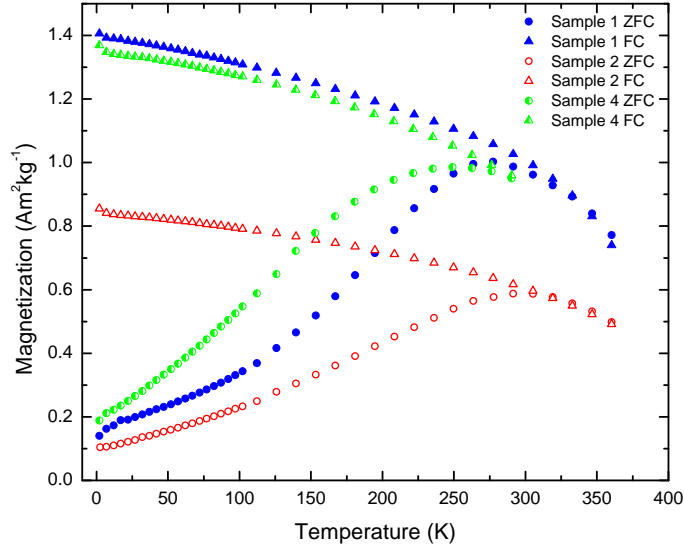
FIGURE 9. Magnetization vs. temperature for samples 1, 2 & 4 at 2.5 mT. All samples have a similar behaviour and each show a blocking temperature, which taken as being the temperature of the maximum in the ZFC curves. Values for the blocking temperatures of each sample are given in Table 3.

[24, 25]. Using a CeO_2 matrix Abiade *et al* [24] were able to show that small nanoparticles (8 nm) could be tuned to have a T_B higher then room temperature and that this was related to the interparticle spacing. Recent work on flower-like maghemite nanoparticles showed that the blocking temperature of iron oxide nanoparticles could be greatly enhanced if mutli-core particles were created [26, 27]. It was thought that magnetic exchange between the surfaces of each particle led to an overall increase in magnetic anisotropy and a hardening of the particles. However dipole-dipole interactions between particles have been shown to also lead to large increases in the blocking temperature which correlated to the increasing particle size within an α-Fe nanoparticulate system where when d=8.32 nm, T_B was enhanced to over 500 K [28]. It is also worth noting that T_B was observed to increase as the degree of crystallinity of the matrix increases [25]. This supports the observation that sample 2 has the highest T_B and suggests that sample 4 has the lowest degree of crystallinity of the matrix. However, it is clear in Fig. 2.1, 3.1 and 5.1, that the nickel nanoparticles are agglomerated and, being in close proximity, strong magnetic dipolar interactions may be present. These are known to enhance blocking temperatures [29, 30] and also give rise to a 'flattening' of the FC curve below T_B which may otherwise be interpreted as a consequence of a narrow particle size distribution [31]. Thus it may be that both an enhancement of the surface magnetocrystalline anisotropy and inter-particle dipolar interactions are responsible for the enhanced values of T_B in samples 1, 2 and 4.

TABLE 3. Particle sizes, Number Densities and linear susceptibilities (χ) from the Langevin Function fit at 290 K with T_B taken from Figure 9. T_B and particle sizes were calculated from the particle sizes from the Langevin function fit as well as the PXRD data for comparison using Equation 1.

Sample	Observed T_B (K)	Calculated Particle Size From Observed T_B (nm)	Number Density (kg^{-1})	Moment $\langle \mu_i \rangle$ From Langevin Moment (μ_B)	Calculated Particle Size From Langevin Function (nm)	Calculated T_B From PXRD Data (K)	Calculated T_B (K)	χ ($10^{-7}\,\mathrm{m^3kg^{-1}}$)
1	281.8	27.85	1.37 x 10^{19}	22315.7	7.49	3.12	1.57	1.11
2	295.6	28.30	1.65 x 10^{19}	24648.5	7.75	3.63	4.05	1.42
4	250.7	26.79	1.77 x 10^{19}	32191.0	8.47	4.55	4.95	2.08

The magnetization vs. applied field data for sample 1 are shown in Fig 10. At 290 K there is a ferromagnetic component that appears to approach a saturation value of approximately 3 Am^2kg^{-1} above about 1 T, however one must consider at this temperature that the only component to be the ferromagnetic particles which may not make up the total nickel mass fraction. At lower temperatures, a second component appears, the magnitude of which increases with decreasing T and it cannot be saturated at 5 T, the highest field achievable in the experiment.
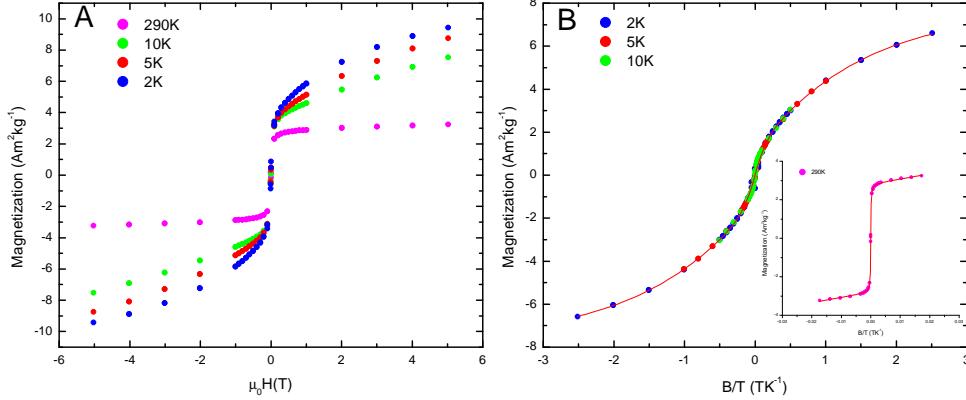

FIGURE 10. **A:** Magnetization vs. applied field for sample 1 (solvent: DCM). **B:** M vs. B/T where once the magnetization from the Langevin component has been subtracted the low temperature data can be scaled onto the 2 K curve. *Inset:* Langevin function and a linear component fit to the 290 K data when plotted as M vs. B/T

The data recorded at 290 K can be fitted with combination of a Langevin function and a linear component (see equation 2). From this linear component we were able to determine the susceptibility of the secondary phase at 290 K to be $1.109 \times 10^{-7} m^3kg^{-1}$.

$$(2) \qquad M = (N\langle\mu\rangle\mu_B) \times \left\{ \coth \frac{\langle\mu\rangle\mu_B B}{k_B T} - \frac{k_B T}{\langle\mu\rangle\mu_B B} \right\} + \chi(T)\frac{B}{\mu_o}$$

Here χ is the mass susceptibility in units of m^3kg^{-1} and $\langle\mu\rangle$ is the mean magnetic moment in units of Bohr magnetons. Parameters obtained from the Langevin Function fits to the data are shown in Table 3, and the particle sizes were calculated from the value of the average magnetic moment along with the room temperature bulk value of the magnetization of nickel (55.2 JT^{-1} kg^{-1} [32]). For the case of sample 1, the particle size of 7.49 nm is the same order of magnitude as the PXRD result of 4.94 nm and, once again, suggests that the TEM image shown in Fig. 2 are likely to be showing clusters of nickel particles rather individual nanoparticles. Similar results were obtained from samples 2 and 4 and the data are given in Table 3.

Fig. 10A also demonstrates the magnetic response of sample 1 at low temperatures. This consists of a paramagnetic response in addition to the ferromagnetic component that was evident at 290 K. In an effort to analyse the low temperature paramagnetic response we computed the forms of the ferromagnetic component using the Langevin function, and the fitting parameters given in Table 3, and we subtracted this from the magnetization measured at 10, 5 and 2 K. Although the Langevin function is not really applicable below T_B it should represent the saturating form of the ferromagnetic magnetization at lower temperatures, and we expect inaccuracies at the lowest values of field. The paramagnetic data obtained from this subtraction were plotted as a function of B/T to scale the results on to a single curve as a test for paramagnetism. However, the data could only be scaled on to a single curve if the value of

the magnetization was corrected with a temperature-dependent scaling factor Sc (see Table 4). The higher temperature datasets were scaled onto the 2 K data, plotted as M vs. B/T as shown in Fig 10B. A fit to the data was performed with the two-term Langevin function shown in equation 3, the Langevin function is a time-independent description of the magnetization above T_B where $J \to \infty$. A single Langevin function would represent a single particle/cluster size however the use of a summation of two indicates that there is a particle size distribution present within the system, in fact, one can use a summation of Langevin functions to describe the magnetization of a system with a large particle size distribution. The parameters that were obtained from the fit to the data of Fig. 10B are shown in Table 4.

$$
\begin{aligned}
M = (N_1 \langle \mu_1 \rangle \mu_B) &\times \left\{ \coth \frac{\langle \mu_1 \rangle \mu_B B}{k_B T} - \frac{k_B T}{\langle \mu_1 \rangle \mu_B B} \right\} \\
+ (N_2 \langle \mu_2 \rangle \mu_B) &\times \left\{ \coth \frac{\langle \mu_2 \rangle \mu_B B}{k_B T} - \frac{k_B T}{\langle \mu_2 \rangle \mu_B B} \right\}
\end{aligned}
$$

(3)

Since the data have been scaled onto the 2 K curve by multiplying by an factor (Sc) affecting only the magnitude of the magnetization it implies that, as the temperature is decreasing, the number of magnetic moments responding to the magnetic field is also decreasing. This may be expected if the system has a ground state where the value of the magnetic moment is zero[4]. This type of behaviour has been reported previously where a Langevin function with a linear term has been fit to particles dispersed in a diamagnetic matrix, where the system should behave superparamagentically but the particle sizes calculated from the magnetic moments of the particles are unrealistic for a Langevin function fit (i.e. sub-nanometer [12]).This is also a similar result to our study of producing Ni nanoparticles from the decomposition of Ni(COD)$_2$ by varying the temperature where a two-term Langevin function is fit to the scaled data but produced particle sizes suggesting sub-nanomater clusters had formed [33].

---

[4]Note that, although we have used a two-term Langevin function (equation 3) to fit to the data, this may only be an empirical fit and not be a true physical representation of the magnetic response of the system.

TABLE 4. Parameters from the two-term Langevin Function fit to the data for all samples. In the case of samples 1, 2 and 4 the results are once the 'ferromagnetic' step modelled by equation 1 has been subtracted from the moment and N are the number densities for each respective particle size. For samples 3 and 5 there was no need to subtract any ferromagnetic/superparamagnetic contribution.

Sample	Moment $\langle \mu_1 \rangle$ (μ_B)	Moment $\langle \mu_2 \rangle$ (μ_B)	N_1 (kg^{-1})	N_2 (kg^{-1})	Particle Size 1 (nm)	Particle Size 2 (nm)	5 K Sc	10 K Sc
1	1.9	20.2	3.95×10^{23}	9.82×10^{21}	0.33	0.73	1.35	1.55
2	1.8	11.5	9.32×10^{23}	4.34×10^{22}	0.32	0.40	1.25	1.35
3	1.7	13.0	1.29×10^{24}	2.59×10^{22}	0.22	0.63	1.638	1.565
4	1.9	14.8	8.60×10^{23}	3.58×10^{22}	0.33	0.65	1.27	1.50
5	2.1	19.1	7.12×10^{23}	2.41×10^{22}	0.34	0.71	1.410	1.565

The results from samples 2 and 4 were similar to those of sample 1 (M vs. H data for samples 2 and 4 are shown in the Supplementary Material). Fits to the 290 K were made with equation 2 and the fitting parameters are given in table 3. The low temperature paramagnetic responses were analysed in the same way as described for sample 1 including a subtraction of the ferromagnetic component (represented as Langevin functions and using N and μ given in table 3), scaling as a function of B/T using the Sc factor and a fit with equation 3. The results of these analyses are also shown in table 4. As with sample 1, the temperature dependent scaling factors suggests that, as the temperature decreases, the numbers of paramagnetic species contributing to the magnetization also appears to decrease.

The $M(B,T)$ data of samples 1, 2 and 4 suggest that initially dissolving the Ni(COD)$_2$ in THF has had an effect on the second magnetic phase of the material. Samples 2 and 4 exhibit a much greater magnetization at 5 T at low temperatures; at 2 K and 5 T both samples 2 and 4 have a magnetization of approximately 15 Am^{2}kg^{-1} where as sample 1 has a magnetization of approximately 6.5 Am^{2}kg^{-1}. However the issue of mass fraction may play a substantial role as noted previously. All three samples show a similar superparamagnetic particle size from the Langevin function fit at 290 K and the extra linear susceptibility components are generally similar (see table 3). Also, the second, low temperature paramagnetic components are qualitatively the same in all three samples where a two term Langevin function can be fit to the scaled data. The fact that all the data scale implies that a similar physical origin to the paramagnetism is applicable to all the samples.

3.2.2. *Samples 3 & 5.*

The two samples both behave paramagnetically at high temperatures as shown in Fig. 11 and, though the solvents used are similar, there is a difference in behaviour of the samples at low temperatures. Sample 5 shows a transition at ∼5 K that may be a blocking temperature associated with the Ni nanoparticles indicated in Fig. 6, though a ≤1 nm particle would suggest a much smaller value of T_{B}. Moreover, the coercive field of the sample must be greater than 2.5 mT (the applied field) at very low temperatures. Sample 3 shows a somewhat different response as, although it appears to be a paramagnetic material, the ZFC and FC curves do not lie on top of one an other. This would generally suggest that there may perhaps be a slight amount of coercivity within the system, however the FC under-shoots the ZFC which is not accounted for by the error within the measurement. This may be explained by solvent evaporation from the sample itself within the magnetometer as a change in the composition of the sample might result in different mass magnetizations at a given field/temperature. Re-plotting the data as χT vs T as shown in figure 11 reveals the complexity of the magnetic responses of both samples. For sample 5, the fall in the value of χT with temperature(decreasing from 300 K) is a characteristic of antiferromagnetic (AFM) interactions [34] between a pair of spins. Moreover, the small peak in χT detected below 20K indicates the presence of small ferromagnetic (FM) interactions at low temperatures [35]. Simple simulations of χT vs T (above 8K) suggested the higher temperature behaviour could be accounted for by an interacting pair of spin 1/2 entities with an exchange constant of about -200 K, while the FM interaction is between higher spin entities; a non-interacting high spin (e.g. S=10) paramagnetic component was also needed to completely describe the experimental data. Figure 11 also includes data from sample 3 and it is seen that both the ZFC and FC are qualitatively similar even though they are offset from one another. Both curves are dominated by a drop in χT below 320 K and, like sample 5, this drop can be modelled with a pair of spin 1/2 AFM exchange couple entities with the FC case requiring an exchange constant of about -200 K while the ZFC curve requires an exchange constant of about -150 K. This implies the proposed solvent loss in sample 3 is having a profound affect on the exchange interaction, as might be expected. Note that both the ZFC and FC data sets show a 'flattening' occurring below 20 K which can be modelled with a small FM interacting component, similar to sample 5, along with a non-interacting high spin component; both of these features reduced in size with the proposed solvent loss. In fact the only qualitative difference between simulations for χT of sample 3 compared to 5 is the need of a fourth component which

corresponded to a small step in the magnetization from zero to a finite value inferred to occur at a temperature of roughly 390 K. It is interesting to note that this latter component does not change with solvent loss.
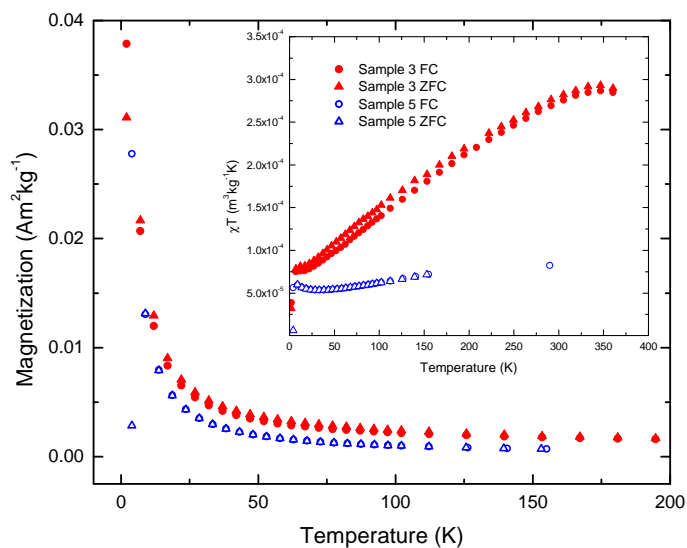

FIGURE 11. Magnetization vs. temperature for samples 3 & 5 at 2.5 mT. Both samples appear paramagnetic at high temperatures however, sample 5 undergoes a transition on the ZFC curve at very low temperatures. *Inset:* χT vs. temperature.
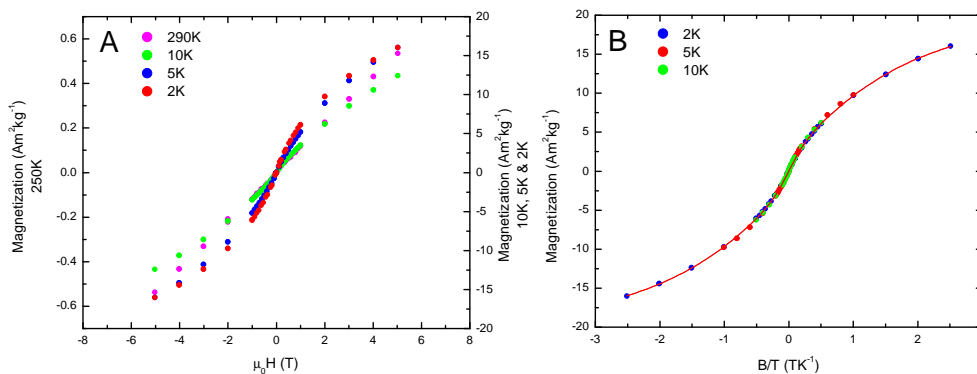

FIGURE 12. **A:** Magnetization vs. applied field **B:** A scaled M vs. B/T plot for sample 3 (solvent: THF/MeCN). The fit to the data is a two-term Langevin function.

The magnetization vs. applied field data for sample 3 are shown in Fig. 12A. The data measured at the 290 K, are linear suggesting a paramagnetic or superparamagnetic response which, according to interpretation of the χT plots mentioned above, would correspond to a response comprising of three paramagnetic components, including AFM coupled spin 1/2 pairs. At low temperatures, a non-linear response of M with B is observed but this is not a simple

paramagnetic behaviour, scaleable by plotting as a function of B/T. However, scaling of the data on to the 2 K data set is possible if the 10 and 5 K data are divided by 1.990 and 1.638 respectively. A 2-term Langevin function (see Equation 3) can be fitted to the data and the parameters obtained from the fit can be seen in Table 4. This form of scaling is the same as that observed for samples 1,2 and 4 and suggests that the low temperature magnetism of sample 3 has a similar origin to those three samples. Sample 5 shows a similar behaviour for the hysteresis loops (see supplementary material) as for sample 3 where the data can be scaled onto one an other when plotted as M vs. B/T. The fitting parameters obtained from this analysis are given in table 4.

4. DISCUSSION

The dielectric constants[5] of the solvents used vary greatly; DCM (8.93), THF(7.52), 1,2-DCB (10.12), MeCN (36.64) and PhCN (25.90) [36, 37]. $Ni(COD)_2$ is decomposed catalytically by halocarbons so it is no surprise that, in the presence of DCM or DCB, the material falls apart and results in the formation of Ni nanoparticles [38, 39]. The solvent THF works well in stabilising $Ni(COD)_2$ and creating a stable solution of Ni(0) should allow the $TCNQF_4$ to undergo a redox reaction with the nickel atoms resulting in a metal-organic compound. The results of samples 2 and 4 demonstrate that when using a halocarbon solvent, regardless of the inclusion of THF within the reaction, Ni particles of a substantial size are formed from the decomposition of $Ni(COD)_2$. The inclusion of THF in the reaction mechanism results in similar particle sizes to sample 1 though the additional component for both samples 2 and 4 have a higher susceptibility as shown from the susceptibilities calculated from the 290 K M vs. H data (see Table 3). This indicates that, by simply including the THF, more of the additional magnetic component is produced than in sample 1 and this component may be simply Ni clusters [33]. Alternatively, the enhancement of this additional component may be due to the fact that the THF is stabilising the $Ni(COD)_2$ for long enough to allow the reduction of the $TCNQF_4$ molecule resulting in a $Ni(II)$-$TCNQF_4$ compound that forms part of the organic matrix. The low angle powder diffraction data (see Fig. 7) of sample 2 suggest that a crystalline phase exists with a larger lattice constant than nickel (the lowest angle feature suggests $d = 5.6$ Å) and is typical of $TCNQF_4$-based solids. The low angle PXRD data of sample 1 and, to lesser extent, sample 4 also suggest the existence of very broad diffraction peaks. Thus it may by simply adding THF to DCM has, in sample 2, has enhanced the crystallinity over that exhibited by sample 1, perhaps by slowing down the reaction sufficiently to allow small crystallites to form . However, using THF with the increased polarity solvent, DCB, resulted in poorly resolved diffraction peaks at small angles perhaps suggesting a more rapid reaction leading to an amorphous material or very small crystallites.

Isonitrile solvents result in systems (samples 3 & 5) that show somewhat different magnetic properties compared to samples 1,2 and 4. The isonitrile molecules are extremely good coordinating ligands as they can donate the lone-pair on the nitrogen of the cyano-group and they have an ability to stabilise a negative charge. There are many examples of divalent Ni that form crystals where there are coordinating isocyanide ligands such as acetonitrile [40, 41]. It is also possible to use isocyanide ligands to stabilise zero-valent Ni atoms where $Ni(COD)_2$ has been used as a starting material and, simply by reacting with the isocyanide molecule in a solvent, under an inert atmosphere, one can obtain a stable Ni(0) compound [42]. Molecules similar to benzonitrile have been used in synthetic routes to create stable Ni(0) compounds where $Ni(COD)_2$ is again used as the source of Ni(0); slow addition of the ligand to a $Ni(COD)_2$ solution resulted in an isocyano-Ni(0) stable compound [43, 44].

The remarkable difference between samples 1, 2 & 4 and samples 3 & 5 with varying solvent has a precedent in Miller and Epstein's work on $V(TCNE)_x \cdot y$(solvent) where they saw a dramatic reduction in transition temperature when using more polar solvents [3, 4]. However, in our samples we attribute the dominant magnetic component at low fields to be a result of bulk

---

[5]The dielectric constant is a good indicator of the polarisability and polar nature of the solvent molecule

Ni or Ni nanoparticles/clusters which are most prominent in samples 1, 2 & 4. When looking at the values for the magnetization at $B_{app} = 5$ T for all the samples, except sample 1, the magnetization is of the same order of magnitude and similar values, especially once the Langevin-step function has been subtracted suggesting that despite the overall nickel nanoparticles mass being different the matrix is largely very similar with regards to elemental content. This implies that using THF as a precursor results in more of the additional magnetic component component, dominant at lower temperatures, being created. This additional component may be a result of Ni clusters (i.e. subnanometer) or a metal-organic compound similar to the $V(TCNE)_x$ that has a large amount of structural disorder but behaves as a ferromagnetic material at low temperatures [21, 33]. The disorder may be due to co-ordination of the spineless solvent molecules within the structure replacing possible sites for the $TCNQF_4$ molecules and creating a disruption in the exchange pathway.

It may also be possible for the isocyano solvents to stabilise the Ni(0) atoms through bonding of the electron rich cyano-groups to the atom or atomic cluster making it less favourable for the Ni to form larger nanoparticles and creating atomic clusters with a distorted surface that allows for further bonding of isocyano ligands to the surface. Opening the reaction mixture to air, as was done by Jain *et al* [5] in Ni_2TCNQ, may result in the decomposition of these stable Ni(0)-isocyano compounds or atomic clusters. It may be that $TCNQF_4$ may also be reduced by the surface of the Ni atomic clusters rather than individual Ni(0) atoms and the cyano-group on the $TCNQF_4$ may act as an effective stabilising surface ligand. If one uses an isocyanide solvent this may result in the surface of the Ni clusters being stabilised by the spinless solvent, acting as a non-magnetic spacer molecule, rather then the $TCNQF_4$ which would create more disorder and disrupt the magnetic exchange pathways between particles causing the overall blocking temperature to decrease.

The work of Finney and Finke on nanocluster nucleation and growth suggest that a four step double autocatalytic mechanism may be present within our system, where the zero-valent transition metal self-assembles to give bulk metal particles [45, 46]. They concluded that as well as being four mechanistic steps each with its own rate constant, low concentrations and high temperatures are used to favour the creation of nanoclusters as opposed to larger particles. Finney and Finke also extended their research to look at the kinetics of the autocatalytic decomposition reaction with varying reaction conditions [47]. They reported that the products of the metal reduction reaction can be changed from bulk metal to nanoclusters depending on the choice of solvent. By using a more polar solvent (propylene carbonate vs. acetone) Finney and Finke showed that the auto-catalytic decomposition reaction resulted in smaller nanoclusters rather than the bulk transition metal [47]. They presumed that the more polar solvent is a more effective stabilizer and slows down the rate of agglomeration. This is especially important when the solvent can also be a stabilising ligand and it has been predicted that solvents with higher dielectric constants are more effective as a ligand [48]. One example of a purely solvent stabilised system is work by Reetz and Lohmer where they showed that Pd nanoclusters could be stabilised by the propylene carbonate solvent molecules [49]. However recent work by Finke's research group presented results that did not fit with solvent-only stabilised nanoclusters where anion coordination was also needed to form Ir nanoclusters rather then bulk metal. What was observed was that solvents with a higher dielectric constant coupled with the existence of an anion, in their case $[BF_4]^-$, lead to dispersed nanoclusters in solution where as using a less polar solvent and counter anion gave bulk metal particles [50]. We believe that, within the $Ni(COD)_2$ and $TCNQF_4$ reaction, using more polar solvents has created a similar effect to that observed by Finney and Finke, where the high dielectric constant solvents produce nanoclusters; this effect is clearly pronounced in the difference between samples 3 and 5. However it may also be that the $TCNQF_4$ anion is also included in stabilising the nanoclusters similar to Starkey, Ott and Finke's recent work. To confirm this more work is needed on the decomposition reaction of $Ni(COD)_2$ in the presence of a strong electron acceptor with different polarity solvents as the reaction medium.

5. CONCLUSION

We have synthesised five samples where the nanoparticle size and distribution can be controlled simply by varying the reaction solvents. Using only DCM as the solvent (sample 1) similar to Jain *et al* [5] creates a material that has two clear magnetic components; one that is superparamagentic Ni nanoparticles and a metal/organic based matrix. By initially dissolving the Ni(COD)$_2$ in THF, the zero-valent Ni atoms are stabilized and using halocarbon solvents (samples 2 and 4) also produces Ni nanoparticles but the blocking temperature can be controlled by varying the polarity of the solvent. From our TEM and PXRD data it is clear that the particles are Ni rich and they agglomerate together, where the average particle size is small (< 10 nm). The particle size was also confirmed by our room temperature magnetic measurements. Interestingly when the blocking temperature is calculated for these nanoparticles it is much lower than what we observed which suggests that either the matrix may have a significant role in hardening the magnetic response of these nanoparticles or magnetic dipole-dipole interactions are strong enough to raise T_{B} [30]. Low temperature M vs. H curves can be fit to a two-term Langevin function which may suggest the presence of a distribution of particle sizes. The mean magnitude of the magnetic moment obtained from this fit indicates that the magnetic response may actually be from atomic clusters. This is similar to our conclusions drawn from an investigation the magnetic properties of Ni(COD)$_2$ [33] which also suggested the presence of Ni clusters within an organic based matrix. Nevertheless, it may be that in our Ni$_x$TCNQF$_4$ samples also contain a stoichiometric metal-organic phase that displays antiferromagnetic properties, like that observed in samples 3 and 5, and as T decreases and this acts as a medium for magnetic exchange to harden the magnetic response of the Ni nanoparticles which increases their blocking temperature.

We have found that using a nitrile based solvent, as well as THF, leads to very small, well dispersed particles that behave similarly to paramagnetic systems. However, our results from sample 5 may be interpreted as indication of the presence of a blocking temperature at low temperatures, or indeed as exhibiting another type of magnetic transition. The particles detected in samples 3 and 5 do not appear to behave in a superparamagnetic fashion at the lowest temperatures and the data from the M vs. B/T can be scaled onto the 2 K data set and a two term Langevin function can be fitted to the data in an analogous fashion to the second phase of Samples 1, 2 and 4. Essentially we have created a material with a magnetic response that resembles the matrix of samples 1,2 and 4.

In general, we have been able to control the both the nanoparticle size and the matrix by simple variation of the solvent with the reaction of Ni(COD)$_2$ and TCNQF$_4$. When using a nitrile based solvent we are able to create very small well dispersed atomic clusters within an organic based matrix, however when using a halocarbon based solvent it is possible to create Ni nanoparticles within a matrix that exhibits a much higher blocking temperature and thus magnetic anisotropy than what is usually expected for nickel particles of a similar size.

6. ACKNOWLEDGMENTS

REFERENCES

[1] J. Manriquez, G. Yee, R. McLean, A. Epstein and J. Miller. A Room-Temperature Molecular Organic Based Magnet. *Science* **252** (1991) 1415-1417

[2] P. Zhou, S. M. Long, J. S. Miller and A. J. Epstein. Static magnetic properties and critical behaviour of V(TCNE)$_x \cdot y$(C$_4$H$_8$O), a high T$_C$ molecular based magnet. *Phys. Letts. A.* **181** (1993) 71-79

[3] P. Zhou, B. G. Morin, J. S. Miller and A. J. Epstein. Magnetization and static scaling of the high-T$_C$ disordered molecular-based magnet V(TCNE)$_x \cdot y$(CH$_3$CN) with $x \sim 1.5$ and $y \sim 2$. *Phys. Letts. A.* **181** (1993) 71-79

[4] P. Zhou, B. G. Morin, J. S. Miller and A. J. Epstein. Complex ac susceptibility studies of the disordered molecular based magnets V(TCNE)$_x$: Role of spinless solvent. *J. Appl. Phys.* **73** 10 (1993) 5648-5650

[5] R. Jain, K. Kabir, J. B. Gilroy, K. A. R. Mitchell, K. Wong and R. G. Hicks. High-Temperature Metal-Organic Magnets. *Nature* **445** (2007) 291-294

[6] J. S. Miller and K. I. Pokhodnya. Formation of Ni[C-4(CN)(8)] from the reaction of Ni(COD)(2) (COD=1,5cyclooctadiene) with TCNE in THF. *J. Mater. Chem.* **17** (2007) 3585-3587

[7] G. Wilke. Contributions to Organo-Nickel Chemistry. *Ange. Chem. Int. Ed. Engl.* **27** 1 (1988) 185-206

[8] K. S. Suslick Sonochemistry. *Science* **247** 4949 (1990) 1439-1445

[9] Y. Koltypin, A. Fernandez, T. C. Rojas, J. Campora, P. Palma, R. Prozorov and A. Gedanken. Encapsulation of nickel nanoparticles in carbon obtained by the sonochemical decomposition of Ni(C8H12)(2). *Chem. Mater.* **11** 5 (1999) 1331-1335

[10] P. B. Oliete, T. C. Rojas, A. Fernandez, A. Gedanken, Y. Koltypin and F. Palacio. Characterisation and magnetic behaviour of nickel nanoparticles encapsulated in carbon. *Acta. Mater.* **52** 8 (2004) 2165-2171

[11] O. Petracic. Superparamagnetic nanoparticle ensembles *Superlattice Microst.* **47** 5 (2010) 569-578

[12] X. Chen, S. Bedanta, O. Petracic, W. Kleemann, S. Sahoo, S.Cardoso and P. P. Freitas. Superparamagnetism versus superspin glass behaviour in dilute magnetic nanoparticle systems. *Phys. Rev. B.* **72** 21 (2005) 214436

[13] M. Bandyopadhyay and S. Dattagupta. Memory in nanomagnetic systems: Superparamagnetism versus spin-glass behaviour Memory in nanomagnetic systems. *Phys. Rev. B.* **74** (2006) 1-5

[14] K. J. Quinn. *Masters Thesis* Durham University (2009)

[15] A. Ceylan, C. C. Baker, S. K. Hasanain and S. I. Shah. Nonmonotonic concentration dependence of magnetic response in Fe nanoparticle-polymer composites *Phs. Rev. B* **72** (2005) 134411

[16] A. L. Patterson. The Scherrer Formula for X-Ray Particle Size Determination. *Phys. Rev* **56** (1939) 978-982

[17] T. J. Emge, M. Maxfield, D. O. Cowan and T. J. Kistenmacher. Solution and Solid State Studies of Tetrafluoro-7,7,8,8- Tetracyano-p-Quinodimethane, TCNQF$_4$. Evidence for Long- Range Amphoteric Intermolecular Interactions and Low- Dimensionality in the Solid State Structure *Mol. Cryst. Liq. Cryst.* **65** 3 (1981) 161-178

[18] T. H. Le, A. Nafady, J. Lu, G. Peleckis, A. M. Bond and L. L. Martin. Electrochemical Synthesis and Characterization of Semiconducting Ni(TCNQF4)$_2$(H2O)$_2$ (TCNQF4 = 2,3,5,6-tetrafluoro-7,7,8,8- tetracyanoquinodimethane) *Eur. J. Inorg. Chem.* (2012) 2889-2897

[19] T. H. Le, A. Nafady, A. M. Bond and L. L. Martin. Electrochemically Directed Synthesis of Co^{2+} and Ni^{2+} Complexes with TCNQF4^{2-} (TCNQF4 = 2,3,5,6-Tetrafluoro-7,7,8,8-tetracyanoquinodimethane) *Eur. J. Inorg. Chem.* (2012) 5534-5541

[20] H. Zhao, R. A. Heintz, X. Ouyang, K. R. Dunbar, C. F. Campana and R. D. Rogers. Spectroscopic, Thermal, and Magnetic Properties of Metal/TCNQ Network Polymers with Extensive Supramolecular Interactions between Layers *Chem. Mater.* **11** 3 (1999) 736-746

[21] R. Clerac, S. O'Kane, J. Cowen, X. Ouyang, R. Heintz, H. H. Zhao, M. J. Bazile and K. R. Dunbar. Glassy magnets composed of metals coordinated to 7,7,8,8-tetracyanoquinodimethane: M(TCNQ)(2) (M = Mn, Fe, Co, Ni). *Chem. Mater.* **15** 9 (2003) 1840-1850

[22] J. J. M. Franse. Magnetic Anisotropy in Nickel and Iron; The Effect of Pressure. *J. Phys. Colloques* **32** Cl (1971) 186 - 192

[23] S. Blundell. Magnetism in Condensed Matter Oxford University Press (2001)

[24] J. T Abiade, S. Ho Oh, D. Kumar, M. Varela, S. Pennycock, H. Guo, A. Gupta and J. Sankar. The effect of matrix and substrate on the coercivity and blocking temperature of self-assembled Ni nanoparticles *J. Appl. Phys.* **104** (2008) 073910

[25] D. Kumar, H. Zhou, T. K. Nath, A. V. Kvit and J. Narayan. Self-assembled epitaxial and polycrystalline magnetic nickel nanocrystallites *Appl. Phys. Lett.* **79** (2001) 17 2817-2819

[26] L. Lartigue, P. Hugounenq, D. Alloyeau, S. P. Clarke, M. Lévy, J. Bacri, R. Bazzi, D. F. Brougham, C. Wilhelm and F. Gazeau. Cooperative Organization in Iron Oxide Multi-Core Nanoparticles Potentiates Their E?ciency as Heating Mediators and MRI Contrast Agents newblock*ACS Nano* **6** (2012) 10935

[27] P. Hugounenq, M. Lévy, D. Alloyeau, L. Lartigue, E. Dubois, V. Cabuil, C. Ricolleau, S. Roux, C. Wilhelm, F. Gazeau and R. Bazzi Iron Oxide Monocrystalline Nanoowers for Highly E?cient Magnetic Hyperthermia *J. Phys. Chem. C.* **116** (2001) 15702

[28] H. Kura, M. Takahashi and T. Ogawa. Extreme enhancement of blocking temperature by strong magnetic dipoles interaction of ?-Fe nanoparticle-based high-density agglomerate *J. Phys. D: Appl. Phys.* **44** (2011) 022002

[29] S. Tomita, P.E. Jonsson, K. Akamatsu, H. Nawafune, and H. Takayama. Controlled magnetic properties of Ni nanoparticles embedded in polyimide films *Phys. Rev. B* **76** (2007) 174432

[30] H. Kura, M. Takahashi, and T. Ogawa. Extreme enhancement of blocking temperature by strong magnetic dipoles interaction of α-Fe nanoparticle-based high-density agglomerate *J. Phys. D: Appl. Phys.* **44** (2011) 022002

[31] J.M. Vargas, W.C. Nunes, L.M. Socolovsky, M. Knobel, and D. Zancher. Effect of dipolar interaction observed in iron-based nanoparticles *Phys. Rev. B* **72** (2005) 184428

[32] C. Kittel. Introduction to Solid State Physics 8th Ed. John Wiley & Sons (2004)

[33] A. Berlie, I. Terry and M. Szablewski. A Magnetic Study of Low Moment Nickel Clusters Formed From The Solid-State Decomposition of Nickel Bis-1,5-cyclooctadiene. *J. Cluster Sci.* (2013) DOI:10.1007/s10876-013-0597-9

[34] J. S. Smart. Magnetism eds. G. T. Rado and H. Suhl, Academic Press, New York, **3** (1963) 63-114

[35] O. Kahn. Molecular Magnetism VCH, New York (1993)

[36] J. G. Stark and H. G. Wallace. Chemistry Data Book John Murray; Student international edition edition (1970)

[37] D. R. Lide. CRC Handbook of Chemistry and Physics 87th Edition CRC Press (2006)

[38] R. A. Schunn, S. D. Ittel and M. A. Cushing. Bis(1,5-Cyclooctadiene) Nickel (0) *Inorg. Synth.* **28** (1990) 94-98

[39] C. A. Tolman, D. W. Reutter and W. C. Seidel. A Calometric study of steric effects in the reactions of phosphorus ligands with $Ni(COD)_2$. *J. Organomet. Chem.* **117** (1976) C30

[40] A. Getsis and A Mudring. Tetrakis(acetonitrile)-dibromo-nickel(II), $[Ni(CH_3)_4Br_2]$. *Z. Anorg. Allg. Chem.* **634** (2008) 2130-2132

[41] A. Getsis and A Mudring. Tetrakis(acetonitrile)-dibromo-nickel(II)-di-acetonitrile, $[Ni(CH_3)_4Br_2]\cdot2CH_3CN$. *Z. Anorg. Allg. Chem.* **634** (2008) 619-621

[42] S. D. Ittel. Complexes of Ni(0). *Inorg. Synth.* **28** (1990) 99-104

[43] C. L. Perrine, M. Zeller, J. Woolcock, T. M. Styranec and A. D. Hunter. Structural studies of two isoelectronic tetrakis isocyano complexes. *J. Chem. Crystallogr.* **40** (2010) 289-295

[44] S. Otsuka, T. Yosida and Y. Tatsuno. Isocyanide-nickel(0) and palladium(0) complexes involving unsaturated ligands. *J. Am. Chem. Soc.* **93** 24 (1971) 6462-6469

[45] C. Besson, E. F. Finney and R. G. Finke. Nanocluster nucleation, growth and then agglomeration kinetic and mechanism studies: A more general, four-step mechanism involving double autocatalysis. *Chem. Mater.* **17** (2005) 4925-4938

[46] E. F. Finney and R. G. Finke. Nanocluster nucleation and growth kinetic and mechanistic studies: A review emphasising transition-metal nanoclusters *J. Colloid Interface Sci.* **317** (2008) 351-374

[47] E. F. Finney and R. G. Finke. The four-step, double-autocatalytic mechanism for transition-metal nanocluster nucleation, growth and then agglomeration: Metal, ligand, concentration, temperature and solvent dependency studies. *Chem. Mater.* **20** (2008) 1956-1970

[48] L. Starkey Ott and R. G. Finke. Transition-metal nanocluster stabilization for catalysis: A critical review of ranking methods and putative stabilizers *Coord. Chem. Rev.* **251** (2007) 1075-1100

[49] M. T. Reetz and G. Lohmer. Propylene carbonate stabilized nanostructured palladium clusters as catalysts in Heck reactions *Chem. Commun.* **16** (1996) 1921-1922

[50] L. Starkey Ott and R. G. Finke. Nanocluster formation and stabilization fundamental studies: Investigating "solvent only" stabilization en route to discovering stabilization by the traditionally weakly coordinating anion BF_4^- plus high dielectric constant solvents. *Inorg. Chem.* **45** (2006) 8382-8393